

Frozen magma lenses below the oceanic crust

Mladen R. Nedimović¹, Suzanne M. Carbotte¹, Alistair J. Harding², Robert S. Detrick³, J. Pablo Canales³, John B. Diebold¹, Graham M. Kent², Michael Tischer¹ & Jeffrey M. Babcock²

The Earth's oceanic crust crystallizes from magmatic systems generated at mid-ocean ridges. Whereas a single magma body residing within the mid-crust is thought to be responsible for the generation of the upper oceanic crust, it remains unclear if the lower crust is formed from the same magma body, or if it mainly crystallizes from magma lenses located at the base of the crust^{1–3}. Thermal modelling^{4–6}, tomography⁷, compliance⁸ and wide-angle seismic studies⁹, supported by geological evidence^{3,10–18}, suggest the presence of gabbroic-melt accumulations within the Moho transition zone in the vicinity of fast- to intermediate-spreading centres. Until now, however, no reflection images have been obtained of such a structure within the Moho transition zone. Here we show images of groups of Moho transition zone reflection events that resulted from the analysis of ~1,500 km of multi-channel seismic data collected across the intermediate-spreading-rate¹⁹ Juan de Fuca ridge. From our observations we suggest that gabbro lenses and melt accumulations embedded within dunite or residual mantle peridotite are the most probable cause for the observed reflectivity, thus providing support for the hypothesis that the crust is generated from multiple magma bodies.

The Moho transition zone (MTZ), located at the crust–mantle boundary, separates layered gabbros of the crust (derived by magma crystallization) from residual peridotites (generally harzburgites) representing mantle rocks^{10,12}. Mapping of the Oman and the Bay of Islands ophiolite complexes, both of which are inferred to be composed of obducted oceanic lithosphere formed at intermediate- to fast-spreading ridges, has shown that the MTZ is composed of sills and lenses of gabbro intruded into dunite or, occasionally, into harzburgite^{3,10–18}. The thickness of the MTZ can vary from a few metres to over two kilometres^{10,12}. A thin MTZ (<~100 m)¹⁷ is widespread within the mapped ophiolites and is characterized by intense deformation resulting from solid-state flow away from the ridge axis that transposes all lithologic units into parallelism sub-horizontal to the Moho. In the few areas where a localized, thick MTZ (>~100 m)¹⁷ is observed, individual gabbro sills and lenses can reach thicknesses of a few hundred metres¹². Locally steep orientation of foliation planes and lineations within high-temperature peridotite led to the association of thick MTZs of the Oman ophiolite with preserved ancient mantle diapirs, many of which are centred along inferred palaeo-ridge axes¹⁶. Gabbro sills of the thick MTZ display strong magmatic flow structure, with lineations and foliations parallel to those within the surrounding peridotites where solid-state conditions prevailed. These structures were formed during the horizontal flow, carrying upper mantle formations away from the ridge axis¹³.

In our Juan de Fuca reflection sections, the Moho discontinuity is imaged along more than 60% of the survey track (Fig. 1). Because the inferred crustal thickness is remarkably uniform, as inferred from two-way travel times ($2,080 \pm 100$ ms), the stratigraphic level of

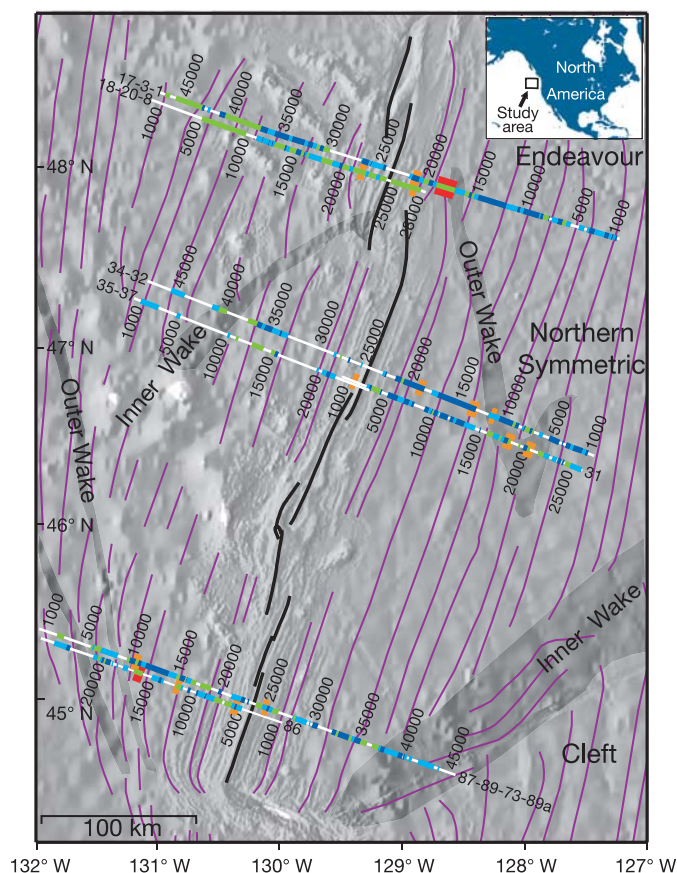


Figure 1 | Study area and strength of the Moho reflection event for the 2002 Juan de Fuca ridge flank seismic profiles is plotted in colour over a sun-illuminated grey bathymetry map. The following reflection strength colour code was used: strong Moho reflection (dark blue); moderate Moho reflection (bright blue); weak Moho reflection (green); no Moho reflection (white). From north to south, seismic profiles cross Endeavour, Northern Symmetric and Cleft ridge segments. Every 5,000th common midpoint (CMP), corresponding to a distance of 31.25 km, is annotated along each profile. Thick red and orange line segments mark sections characterized by sub-Moho reflection events. The MTZ reflection events marked in red were imaged at a high signal-to-noise ratio. The interpreted traces of the ridge axis are indicated with thick black lines and magnetic isochrons¹⁹ with thin purple lines. Overlay areas approximately outline the location of inner and outer propagator wakes. The inset shows the location of the study area with respect to North America.

¹Lamont-Doherty Earth Observatory of Columbia University, 61 Route 9W, PO Box 1000, Palisades, New York 10964-8000, USA. ²Scripps Institution of Oceanography, University of California, San Diego, 9500 Gilman Drive, La Jolla, California 92093-0225, USA. ³Woods Hole Oceanographic Institution, 360 Woods Hole Rd, Woods Hole, Massachusetts 02543-1542, USA.

events originating within the MTZ is well constrained. The Moho discontinuity is mostly represented by a single reflection event of variable strength, at places remarkably sharp and strong (Fig. 2a). Seismic modelling studies^{11,20} suggest that areas with a single strong or moderately strong Moho reflection event are probably characterized by an abrupt passage from layered gabbros of the lower crust, to residual peridotites of the uppermost mantle. Areas with weak or no Moho reflection event may be indicative of rough Moho topography that scatters acoustic energy, or may represent thick MTZs composed of thin alternating gabbro and dunite sills, where the ratio of dunite to gabbro gradually increases with depth resulting in a gradual downward velocity increase (Supplementary Discussion 1).

In Fig. 2b, we show the largest and the most prominent group of MTZ reflection events recorded (Supplementary Discussion 2). These sub-horizontal reflections are located on line 17-3-1, more than 30 km east of the ridge axis (Fig. 1). The Moho reflection event in this section of line 17-3-1 is weak but traceable, placing the recorded events just below the crust. For the purposes of discussion and following ref. 12, we assume that the geophysical Moho and petrological Moho are equivalent, and that the MTZ is therefore the uppermost part of the mantle. The spatial character of the imaged

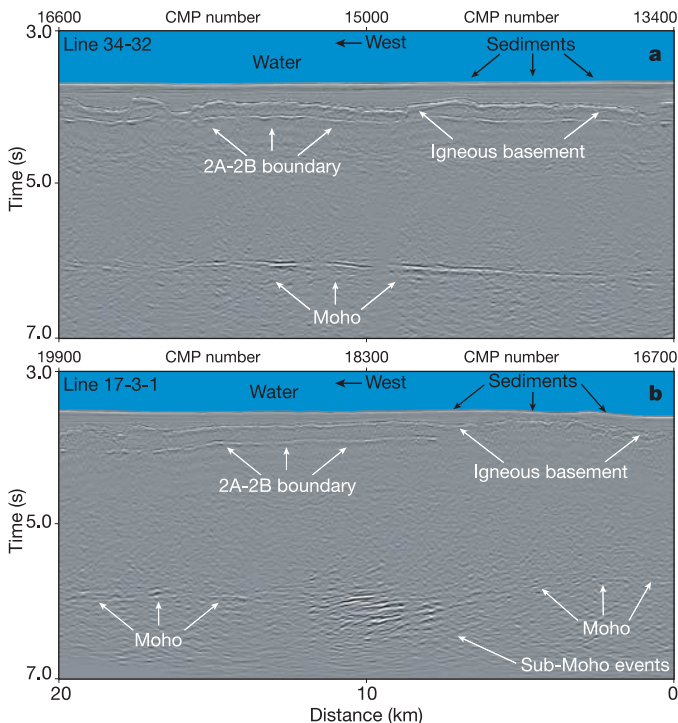


Figure 2 | Seismic reflection structure of the oceanic crust characterized by thick and thin MTZs. **a, b**, Shown are two 20 km-long sections, one of line 34-32 reflection image (**a**) and the other of line 17-3-1 reflection image (**b**), using greyscale variable density plots. The distance to depth ratio is approximately 1:1. Oceanic crustal structure in both sections is imaged remarkably well. Panel **a** is characterized by a mostly continuous and sharp image of the igneous basement surface, the layer 2A/2B boundary and the Moho discontinuity. Panel **b** shows all the same events as panel **a** but differs from it because it also includes a set of sub-Moho reflections, and because it is characterized by a weaker Moho reflection and a layer 2A/2B boundary event that is not imaged across the whole section. Weak events found a few hundred milliseconds below the layer 2A/2B boundary, that may appear to be related to the boundary between the layer 2B and layer 3, are processing artefacts caused by merging of sections with a different content of signal frequencies (2–7–100–125 Hz). To improve the Moho reflection event, only the low signal frequencies (2–7–20–40 Hz) are kept for the deeper parts of the sections. For details about the data acquisition and processing, see Supplementary Methods 1 and 2.

subcrustal reflection events is in excellent agreement with the geometry of the thick MTZ as described by ophiolite studies¹². The anomalous MTZ area is approximately 10 km wide, with individual bright events showing 4–5 km of lateral continuity and a combined thickness of over 2,000 m in the central region, comparable to the maximum thickness mapped in ophiolites^{10,12}.

High signal-to-noise ratio of the imaged MTZ events presented in the migrated stack of Fig. 2b indicates that these reflections probably arise at sharp boundaries between layers of significantly different physical properties. The strength of the observed sub-Moho events may also be partially due to constructive interference from the top and the bottom sill reflections. Assuming that the MTZ events are caused by gabbro sills with a P-wave velocity of 7 km s^{-1} , and that the dominant data signal frequency is $\sim 10\text{--}15 \text{ Hz}$, the strongest responses will be generated by gabbro sills with thicknesses from $\sim 50\text{--}150 \text{ m}$, and will be characterized by single reflection events. This is in agreement with the thickness of large gabbro sills mapped in ophiolites. Sills with thicknesses $< \sim 20 \text{ m}$ cannot be imaged because of destructive wave interference. Images of sills with a thickness $> \sim 200 \text{ m}$ will be characterized by paired top and bottom reflection events of opposite polarity, a pattern not observed in our seismic sections.

Insight about the lithologies causing the reflections can in principle be obtained by analysis of reflection amplitude variation as a function of offset or angle of incidence (AVO/AVA). However, the signal-to-noise ratio of our prestack data was much too low for the standard AVO analysis. We therefore computed trace envelopes (Fig. 3a) for a partially stacked super CMP gather positioned over the brightest group of subcrustal reflections from Fig. 2b, and compared them with calculated amplitude curves for rays reflected from the potential rock interfaces of a thick MTZ (Fig. 3b–f) (Supplementary Discussion 3). The observed reflection strength of the MTZ events seems to gradually weaken with the increasing source-receiver offset, with somewhat greater amplitude drop at offsets larger than about 4 km. Based on the relationship between modelled and observed reflection strength curves (red and blue lines in Fig. 3b and c), we speculate that the imaged reflections were generated at contacts between solid gabbro sills and host dunite, a structural relationship frequently observed in the thick MTZs of the Oman ophiolite¹³. We cannot resolve (see Fig. 3) whether the host rock for the gabbro sills is dunite or residual mantle peridotite³.

The possibility that the strongest MTZ reflections in Fig. 3a were generated at the contact between ultramafic host rocks and gabbro-melt, however, cannot be eliminated. Nevertheless, such an interface is less likely because the ridge axis is located at a significant distance westward ($\sim 33 \text{ km}$), and the predicted reflection amplitude fall-off with offset for a dunite–gabbro–melt interface seems more rapid than that observed (Fig. 3b). Moreover, the reflection amplitudes for the dunite–gabbro–melt contact (Fig. 3b) are much larger than for the corresponding solid–solid interface (Fig. 3c), but high signal-to-noise ratio subcrustal reflections are not identified in the prestack data. The graph shown in Fig. 3f indicates that the lower boundary of thick MTZs, usually represented by a transition from dunite to harzburgite, is transparent for reflection imaging.

In addition to the events shown in Fig. 2b, we were able to identify a number of other areas with complex Moho and sub-Moho reflections along our survey track (Supplementary Discussion 4). The distribution of all imaged subcrustal reflection areas extending for at least 3 km is presented in Fig. 1. The identified thick MTZs form two distinct groups: those centred near the ridge axis and those found beyond ($> \sim 20 \text{ km}$), such as the one shown in Fig. 2b. The thick MTZs found near the ridge axis seem to be uniformly and symmetrically distributed across the ridge axis. An example of a series of subcrustal reflection events located less than 10 km from the ridge axis on line 87-89-73-89a is shown in Fig. 4. Although our data do not provide direct constraints on the lithologic nature of the subcrustal interfaces imaged in the vicinity of the ridge axis, ophiolite

studies^{3,15,17} and other geophysical investigations⁷⁻⁹ indicate that gabbro-melt lenses are emplaced in the MTZ near the ridge axis. Therefore, the observed subcrustal reflections, such as those presented in Fig. 4, are more likely to be generated at the interface between ultramafic rocks and gabbro-melt than the subcrustal reflections located farther away from the ridge axis.

Away from the ridge axis ($> \sim 20$ km), the instances of thick MTZs seem to correlate with the location of outer propagator wakes defined by magnetic isochrons (Fig. 1). The general absence of detectable thick MTZs away from the ridge axis, and outside the outer propagator wake area, suggests a highly dynamic environment at the crust-mantle boundary up to a distance of a few tens of kilometres from the spreading centre. Within this area, MTZ gabbro sills and dunite layers both form and can cease to exist. Structural mapping of the Oman ophiolite provides evidence for two possible mechanisms responsible for thinning of the thick MTZs: tectonic stretching and upward magma discharge^{3,17}.

The thick MTZs found $> \sim 20$ km away from the ridge axis, and in particular the largest ones marked in red in Fig. 1, are distinct from the near ridge axis features in size, shape and thickness. Based on their spatial association with the outer propagator wakes, we suggest that these preserved thick MTZs were formed by intrusion of melt into the crust-mantle boundary area within the zone of active

spreading on the propagating ridge segment. At the propagator tips, the spreading breaks into a relatively cool lithosphere that might allow for large magma bodies to be emplaced and solidified. Ophiolite mapping and our data constrain the maximum thickness of emplaced magma bodies to ~ 150 – 200 m, and their maximum diameter to several kilometres. Existence of isolated magma bodies at propagator tips, which appear to have experienced rapid cooling and high fractional crystallization, is supported by the common occurrence of high amplitude magnetic anomalies and high Fe-Ti basalts^{21,22}. Large intrusions of basaltic melt into previously accreted, and therefore older and colder, oceanic lithosphere are also documented in the Maqсад diapir area of the Oman ophiolite^{23,24}, and were associated with the opening of a propagator¹⁸. Two of the imaged thick MTZs (marked red in Fig. 1), characterized by strong reflection events that we believe are indicative of the thick (~ 50 – 150 m) gabbro sills, might also be associated with diapirism linked to opening of the propagators. In both cases the imaged sills appear to have a ridgeward dip and to be located within the newly accreted crust, which itself is characterized by smoothest topography suggesting locally abundant melt supply. Unlike the crust forming the inside wakes, which is rotated and sheared²¹, the crust forming the outer propagator wakes experiences little deformation²² and therefore provides a sheltered environment in which thick MTZs may be preserved. Interestingly, of the three MTZ melt lenses identified along the East Pacific Rise 11° – 13° N area using PmS waves⁹, two are associated with the outer wakes of migrating overlapping spreading centres.

Our evidence suggests that sill emplacement in the MTZ may be a common feature beneath intermediate spreading centres but the sills themselves are short-lived. Only sills within the thick MTZs formed at propagator tips seem to remain preserved after being accreted to outer propagator wakes. The melt lenses forming these thick MTZs

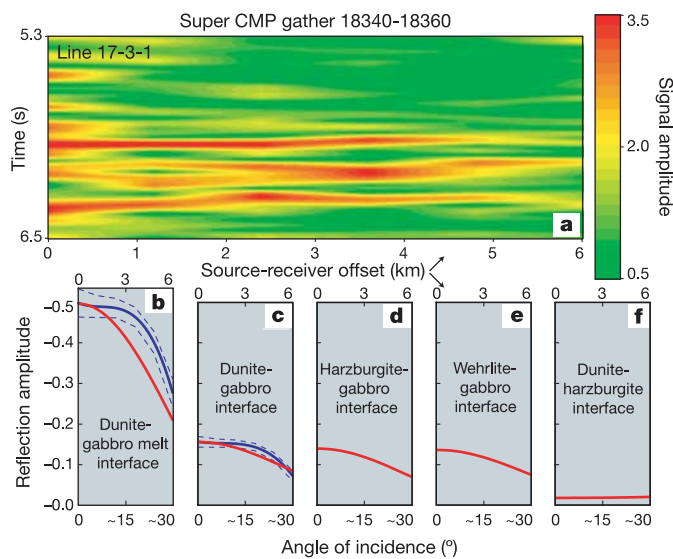


Figure 3 | Modelled and measured reflection amplitude versus offset dependence for the MTZ events shown in Fig. 2b. **a**, Trace envelope of the partially stacked super CMP gather 18340-18360. The super gather is composed of 21 adjacent CMP gathers approximately centred at the middle of the group of bright subcrustal reflection events shown in Fig. 2b. Gather data traces were amplitude corrected only for the geometrical propagation effects and shot and receiver 'surface' inconsistencies, sorted to 1-km-wide partial source-receiver offset gathers and stacked. To estimate the signal reflection strength as a function of arrival time, the partial stacked super gather data were then transformed to trace envelope and plotted in colour. **b-f**, Ray amplitude, in red, as a function of the source-receiver offset for the potential rock interfaces of the thick MTZ shown in Fig. 2b (see Supplementary Methods 3). Lithologic interfaces were formed by superimposing gabbro ($v_p = 7,000 \text{ m s}^{-1}$; $v_s = 3,750 \text{ m s}^{-1}$; $\rho = 2,900 \text{ kg m}^{-3}$), dunite ($v_p = 8,450 \text{ m s}^{-1}$; $v_s = 4,850 \text{ m s}^{-1}$; $\rho = 3,300 \text{ kg m}^{-3}$), harzburgite ($v_p = 8,300 \text{ m s}^{-1}$; $v_s = 4,850 \text{ m s}^{-1}$; $\rho = 3,300 \text{ kg m}^{-3}$), wehrlite ($v_p = 8,100 \text{ m s}^{-1}$; $v_s = 4,650 \text{ m s}^{-1}$; $\rho = 3,300 \text{ kg m}^{-3}$) and gabbro melt ($v_p = 3,200 \text{ m s}^{-1}$; $v_s = 0 \text{ m s}^{-1}$; $\rho = 2,900 \text{ kg m}^{-3}$)^{10,25}. For the inverted interfaces of **b-f**, only the sign (polarity) of the reflection amplitudes changes. Solid and dashed blue lines in **b** and **c** are the cubic fit to the average maximum amplitude for the events shown in **a** and the computed error bounds, respectively. The observed amplitude decay curve is scaled so that it matches **b** and **c** modelled amplitudes at zero-offset.

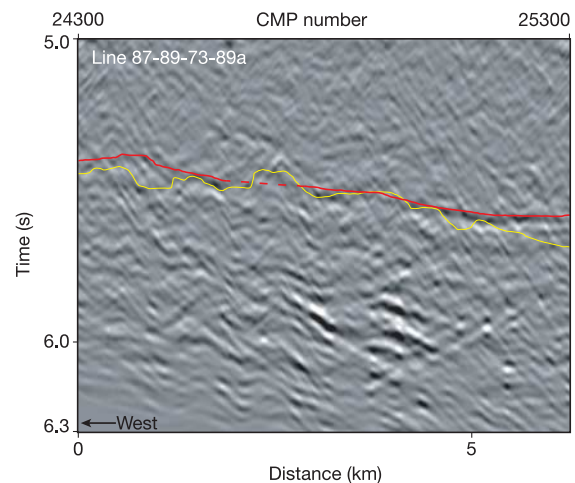


Figure 4 | A series of subcrustal reflection events recorded on line 87-89-73-89a is displayed at the distance to depth ratio of about 1:1. The reflection events are located approximately 7 to 8 km east of the ridge axis (see Fig. 1) and a few hundred milliseconds below the Moho reflection event, which in this section of line 87-89-73-89a is of moderate strength. Our interpretation of the Moho discontinuity location is shown with a continuous red line; dashed yellow line is the igneous basement pick delayed by 2,300 ms, the average two-way travel time through the crust in the vicinity of the Cleft ridge. The presented events appear to exhibit a very mild dip away from the axis but the form and strength of these sub-Moho reflections might be imaged inaccurately due to focusing and defocusing of the acoustic energy in the areas close to the ridge axis, where the seafloor topography is generally rougher. Nevertheless, the recorded signals are probably true sub-Moho reflections as we generally do not observe scattered energy at earlier times, and cannot find an explanation for its focusing just below the Moho discontinuity.

are thought to have experienced repetitious magma expulsion with continuous melt replenishment^{3,15}. Hence, the interpreted large gabbro-melt sills within the thick MTZ shown in Fig. 2b may represent the first images of frozen subcrustal magma chambers.

Received 13 January; accepted 15 June 2005.

- Sinton, J. M. & Detrick, R. S. Mid-ocean ridge magma chambers. *J. Geophys. Res.* **97**, 197–216 (1992).
- Phipps Morgan, J. & Chen, Y. J. The genesis of oceanic crust; magma injection, hydrothermal circulation, and crustal flow. *J. Geophys. Res.* **98**, 6283–6297 (1993).
- Kelemen, P. B. & Aharonov, E. in *Faulting and Magmatism at Mid-Ocean Ridges* (eds Buck, W. R., Delaney, P. T., Karson, J. A. & Lagabriele, Y.) 267–289 (Geophysical Monograph 106, AGU, Washington DC, 1998).
- Garrido, C. J., Kelemen, P. B. & Hirth, G. Variation of cooling rate with depth in lower crust formed at an oceanic spreading ridge: Plagioclase crystal size distributions in gabbros from the Oman ophiolite. *Geochem. Geophys. Geosyst.* **2**, doi:10.1029/2000GC000136 (2001).
- Cherkaoui, A. S. M., Wilcock, W. S. D., Dunn, R. A. & Toomey, D. R. A numerical model of hydrothermal cooling and crustal accretion at a fast spreading mid-ocean ridge. *Geochem. Geophys. Geosyst.* **4**, doi:10.1029/2001GC000215 (2003).
- Maclennan, J., Hulme, T. & Singh, S. C. Thermal models of oceanic crustal accretion: Linking geophysical, geological and petrological observations. *Geochem. Geophys. Geosyst.* **5**, doi:10.1029/2003GC000605 (2004).
- Dunn, R. A., Toomey, D. R., Detrick, R. S. & Wilcock, W. S. D. Continuous mantle melt supply beneath an overlapping spreading center on the East Pacific Rise. *Science* **291**, 1955–1958 (2001).
- Crawford, W. C. & Webb, S. C. Variations in the distribution of magma in the lower crust and at the Moho beneath the East Pacific Rise at 9°–10° N. *Earth Planet. Sci. Lett.* **203**, 117–130 (2002).
- Garmany, J. Accumulations of melt at the base of young oceanic crust. *Nature* **340**, 628–632 (1989).
- Karson, J. A., Collins, J. A. & Casey, J. F. Geologic and seismic velocity structure of the crust/mantle transition in the Bay of Islands ophiolite complex. *J. Geophys. Res.* **89**, 6126–6138 (1984).
- Collins, J. A., Brocher, T. M. & Karson, J. A. Two-dimensional seismic reflection modeling of the inferred fossil oceanic crust/mantle transition in the Bay of Islands Ophiolite. *J. Geophys. Res.* **91**, 12520–12538 (1986).
- Benn, K., Nicolas, A. & Reuber, I. Mantle-crust transition zone and origin of wehrlitic magmas; evidence from the Oman Ophiolite. *Tectonophysics* **151**, 75–85 (1988).
- Boudier, F. & Nicolas, A. Nature of the Moho transition zone in the Oman ophiolite. *J. Petrol.* **36**, 777–796 (1995).
- Boudier, F., Nicolas, A. & Ildefonse, B. Magma chambers in the Oman Ophiolite; fed from the top and the bottom. *Earth Planet. Sci. Lett.* **144**, 239–250 (1996).
- Korenaga, J. & Kelemen, P. B. Origin of gabbro sills in the Moho transition zone of the Oman Ophiolite; implications for magma transport in the oceanic lower crust. *J. Geophys. Res.* **102**, 27729–27749 (1997).
- Nicolas, A., Boudier, F., Ildefonse, B. & Ball, E. Accretion of Oman and United Arab Emirates ophiolite; discussion of a new structural map. *Mar. Geophys. Res.* **21**, 147–179 (2000).
- Jousselin, D. & Nicolas, A. The Moho transition zone in the Oman Ophiolite; relation with wehrlites in the crust and dunites in the mantle. *Mar. Geophys. Res.* **21**, 229–241 (2000).
- Godard, M., Jousselin, D. & Bodinier, J.-L. Relationships between geochemistry and structure beneath a paleo-spreading centre; a study of the mantle section in the Oman Ophiolite. *Earth Planet. Sci. Lett.* **180**, 133–148 (2000).
- Wilson, D. S. Confidence intervals for motion and deformation of the Juan de Fuca Plate. *J. Geophys. Res.* **98**, 16053–16071 (1993).
- Brocher, T. M., Karson, J. A. & Collins, J. A. Seismic stratigraphy of the oceanic Moho based on ophiolite models. *Geology* **13**, 62–65 (1985).
- Hey, R., Duennebie, F. K. & Morgan, W. J. Propagating rifts on midocean ridges. *J. Geophys. Res.* **85**, 3647–3658 (1980).
- Hey, R., Kleinrock, M. C., Miller, S. P., Atwater, T. M. & Searle, R. C. Sea Beam/deep-tow investigation of an active oceanic propagating rift system, Galapagos 95.5 W. *J. Geophys. Res.* **91**, 3369–3393 (1986).
- Ceuleneer, G., Monnerieu, M. & Amri, I. Thermal structure of a fossil mantle diapir inferred from the distribution of mafic cumulates. *Nature* **379**, 149–153 (1996).
- Amri, I., Benoit, M. & Ceuleneer, G. Tectonic setting for the genesis of oceanic plagiogranites; evidence from a paleo-spreading structure in the Oman Ophiolite. *Earth Planet. Sci. Lett.* **139**, 177–194 (1996).
- Carlson, R. L. in *Handbook of Elastic Properties, Liquids, and Gases* (eds Levy, M., Bass, H. & Stern, R.) 377–461 (Academic Press, New York, 2001).

Supplementary Information is linked to the online version of the paper at www.nature.com/nature.

Acknowledgements We are grateful to P. B. Kelemen and W. R. Buck for their reviews. K. Vasudevan provided us with a stacked section of the Canadian line 1989-15, shown in Supplementary Information. The Doherty and National Science Foundations supported this work.

Author Information Reprints and permissions information is available at npg.nature.com/reprintsandpermissions. The authors declare no competing financial interests. Correspondence and requests for materials should be addressed to M.R.N. (mladen@ldeo.columbia.edu).